ACS OMEGA

Open Access

http://pubs.acs.org/journal/acsodf

Article

Stability of Hydroxylated α-Fe_2O_3(0001) Surfaces

Jiachen Chen, Dmitry I. Sharapa, and Philipp N. Plessow*

Cite This: *ACS Omega* 2024, 9, 35449−35457

Read Online

ACCESS | Metrics & More | Article Recommendations | Supporting Information

ABSTRACT: The stability of hydroxylated terminations of the 0001 surface of α−Fe_2O_3 (hematite) is investigated computationally using PBE + U calculations with dispersion corrections. Hydroxylated surfaces with low OH concentrations are found to be most stable in a range of the chemical potential of water of −0.95 eV > μ_{H_2O} > −2.22 eV. These surfaces can be described as isolated $Fe(OH)_3$ groups adsorbed on the dry hematite surface and are predicted to be the exposed termination of the 0001 surface in a wide range of relevant experimental conditions. Most investigated reduced surfaces, containing Fe in oxidation state +2, are only stable in a range of the chemical potential of oxygen μ_O < −2.44 eV, where bulk hematite is less than magnetite. The only reduced surface stable at a higher μ_O is derived from the most stable nonreduced hydroxylated surfaces by removing a single OH group per unit cell.

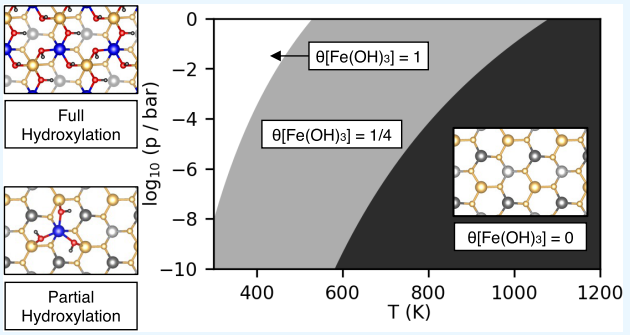

INTRODUCTION

Iron oxides are abundantly available on Earth and are technologically relevant in many areas.[1] The common oxidation states of Fe are +2 and +3, and this leads to the existence of iron oxides with varying composition, where hematite (α−Fe_2O_3) consists only of Fe^{3+}. In catalysis, hematite was investigated as an electrode material for photocatalytic water-splitting, as a catalyst for H_2S-removal,[2−4] and as a precatalyst for CO_2 hydrogenation to hydrocarbons.[5−8] Iron is also discussed as an energy carrier, which can be oxidized to iron oxide using retrofitted coal plants and reduced using green H_2.[9] On an atomic scale, the surface of hematite is one of the central surfaces for the oxidation/reduction processes.[10]

The atomic structure of a surface controls its reactivity and properties. Making reliable predictions using first-principles calculations thus requires the determination of the state of the surface, which is given by the thermodynamically most stable termination, if the system is in equilibrium. Hydroxylation is difficult to determine both experimentally and theoretically, but is known to strongly influence the properties of oxide surfaces.[11] For this reason, many studies have been concerned with determining the most stable termination of the 0001 surface of hematite.[12−19]

Hematite crystallizes in the corundum structure (see Figure 1), and particles with different morphologies can be synthesized or found in nature.[20,21] The stable 0001 facet is found in naturally occurring crystals and has been the subject of many investigations.[22−25] The most stable stoichiometric termination of α-Fe_2O_3(0001) is the (single-metal, or O3-M) terminated surface,[25] which is analogous to α-Al_2O_3.[12,26] This is also referred to as the clean or dry surface, and we will from here on refer to it as the dry surface.

However, in contrast to α-Al_2O_3, hematite can be more easily reduced at the surface, which is also one of the essential properties in its applications. For theoretical investigations, changes in the oxidation state of Fe pose a considerable challenge. For iron oxides, the local density approximation (LDA) and the generalized gradient approximation (GGA) are generally considered insufficient to obtain qualitatively correct results for properties such as the band gap, magnetic moments, and stability and reactivity of surfaces. The computationally most efficient way to tackle these challenges is through a Hubbard-U correction[27−30] applied to the d-electron of the transition metal atoms.

The α-Fe_2O_3(0001) surface was studied computationally in 2004 by Rohrbach et al. using GGA + U calculations.[25] Their study included the stoichiometric single-metal (or O3-M)-terminated surface (same as the dry surface) as well as reduced (oxygen deficient) and oxidized (oxygen enriched) surfaces. As in other investigations,[12,14] their GGA calculations predict oxidized surfaces, where the formal oxidation state of Fe exceeds +3, to be relatively stable. However, ref 25 clearly showed that oxidation of the surface is predicted to be significantly less favorable when using GGA + U with U_{eff} = U − J = 4 eV. Specifically, the chemical potential of oxygen μ_O

Received: March 4, 2024
Revised: May 13, 2024
Accepted: June 4, 2024
Published: August 5, 2024

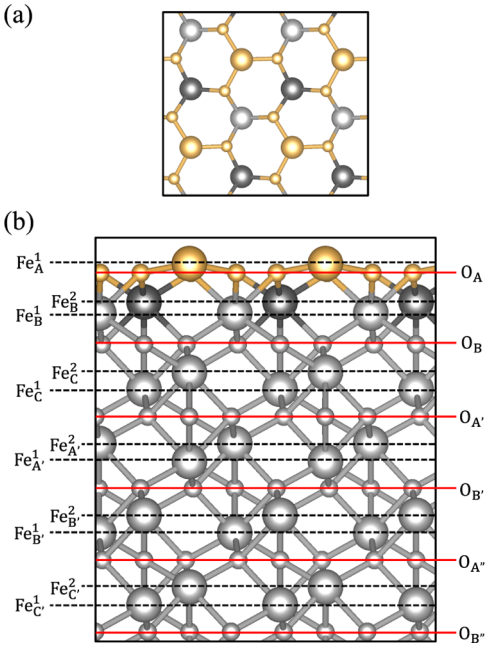

Figure 1. Single Fe-terminated surface model (clean and dry surface). (a) Top view and (b) side view. Letters (A−C) in the lower corner indicate atoms at different layers, and numbers (1, 2) in the upper corner distinguish different atoms in the same layer. Large spheres represent Fe atoms, while small spheres are oxygen atoms.

below which the dry surface becomes more stable than any oxidized surface is shifted from $\mu_O \approx -1.25$ eV to $\mu_O \approx -0.1$ eV for $Fe_2O_3(0001)$ when $U_{eff} = 4$ eV is applied. According to the GGA + U calculations, oxidized α-$Fe_2O_3(0001)$ surfaces (formal oxidation state of Fe > +3) are therefore not expected to form at relevant conditions. Recently, Wang and Hellmann using calculations with the HSE hybrid functional have also found that oxidation of the hematite surface is only viable at very high chemical potentials of oxygen ($\mu_O > -0.25$ eV).[31] It is also noteworthy that the coexistence of surface areas with different terminations was predicted with density functional theory (DFT) for α-$Fe_2O_3(0001)$.[13,32,33]

The existence of ferryl terminations (Fe═O) has been discussed extensively and was proposed based on infrared spectroscopy measurements under mildly oxidizing conditions, for example, 973 K and 2 mbar O_2, corresponding to $\mu_O = -1.2$ eV.[34] However, as indicated above, computational investigations going beyond the GGA level (either GGA + U or hybrid functional) find oxidized structures including ferryl groups to be unfavorable.[16,31] Surface-sensitive X-ray diffraction measurements also indicate the presence of oxygen at the surface of hematite,[11] which may, however, also be present in the form of hydroxyl groups.

In addition to oxidation and reduction, the adsorption of water and the formation of hydroxyl groups play an important role in determining the properties of hydroxylated oxide surfaces.[35] Hydroxylation of hematite surfaces has been observed experimentally using X-ray photoelectron spectroscopy (XPS)[36] and polarization-dependent infrared reflection absorption spectroscopy (IRRAS).[37] Computationally, the adsorption of water on the dry surface and its dissociation were studied extensively.[15,16,37−39] The other main hydroxylated surface that has been studied a lot is the fully hydroxylated surface (Fe−$(OH)_3$-terminated).[31] The interface of hematite with liquid water was also investigated in a number of studies.[40−42] Beyond the well-known dry surface and the fully hydroxylated surface, a vast number of hydroxylated structures have been studied computationally.[15,16,31,37−44] These were typically obtained by cutting the surface at some layer (O_3, Fe, or Fe_2) and adding variable amounts of H or OH groups. Many of the structures generated in this way contain Fe in bonding situations differing from the usual oxidation states (+2 and +3). To our knowledge, there is no known stable hydroxylated structure in between fully hydroxylated and dry surfaces, except defective reduced structures that are only stable at the extremely low chemical potential of oxygen μ_O.

In this work, we investigated the stability of hydroxylated surfaces of α-$Fe_2O_3(0001)$ taking into consideration the structural motifs discovered by us for α-$Al_2O_3(0001)$.[45] In contrast to the approach of cutting the hematite surface and adding H and OH groups, we identify adsorbed $Fe(OH)_3$ as the fundamental building block of the fully hydroxylated surface with $\theta[Fe(OH)_3] = 1$. Lowering the coverage of $Fe(OH)_3$ to $\theta[Fe(OH)_3] = 1/4$ leads to isolated $Fe(OH)_3$ groups, which are more stable at low chemical potential, i.e., at high temperatures and low partial pressures of water. Additionally, we also studied reduced surfaces (Fe in oxidation state +2) with and without hydroxyl groups.

METHODS

PBE + U calculations[27−30,46] were carried out with a value of U = 4 eV and J = 0 eV[47] along with Grimme's D3 dispersion correction (zero damping).[48] The DFT + U method was used in the form proposed by Liechtenstein and Dudarev et al.[27−30] and applied to the d-orbitals of Fe.

The value of the U-parameter can be motivated by empirical fitting to reproduce properties of interest, such as lattice constants, band gaps, or reaction energies. Alternatively, it can be deduced from a linear response calculation according to the underlying theory of DFT + U as a means to correct for the self-interaction error and to achieve the correct behavior of the slope of energy vs number of electrons.[49] Linear response calculations for bulk hematite gave U = 3.81 eV, and for most surfaces and Fe atoms, a value of U in the range between 4 and 5 eV.[50] In a study, where the U values were systematically tested for 3, 4, and 5 eV, it was concluded that 3 eV is best for the overall thermodynamic properties of iron oxides, while 4 eV gives improved band gaps and structures.[51] Our choice of U = 4 eV is therefore a good compromise between an empirical choice of U based on computed properties and results from the linear response approach aiming to fix fundamental shortcomings of the GGA in treating electron correlation. Furthermore, a value of U = 4 eV was used in many previous studies[13,16,25,39,52] and 4.3 eV was used by Hellman and coworkers.[31,53] In addition to the calculations with U = 4 eV which are the basis for the results provided in the main text, single-point calculations with U = 3 and 5 eV were performed and are analyzed in more detail in the Supporting Information (SI).

In addition to the value of U, using a different reference for oxygen is another approach that will change the obtained results. Alternatives to using O_2 as a reference are, for example, using the O atom or (H_2O-H_2) and employing the known experimental formation energies[54] of the O atom (2.558 eV) and H_2O (−2.476 eV). We decided to use the energy of O_2 in its triplet ground state, first and foremost, because this is the common choice of reference state in computational studies on iron oxides[14,25,39,50,51,53,55] and it thus facilitates the compar-

https://doi.org/10.1021/acsomega.4c02113
ACS Omega 2024, 9, 35449−35457

ison with the literature. Second, we do not believe that shifting the oxygen reference provides a general solution (see discussion in the SI). Lastly, based on the results presented here, it is easy to read off what the results would be with a different oxygen reference. In particular, using the O atom as a reference will shift μ_O by +0.43 eV and using H_2O will shift μ_O by +0.20 eV. In both cases, this will make oxygen more reactive, i.e., it will make the formation of reduced α-Fe_2O_3 surfaces less favorable.

DFT calculations in this study were performed using the projector-augmented wave (PAW) method, standard PAW potentials, and a kinetic energy cutoff of 600 eV for the wave function expansion in plane waves. The VASP software package (version 5.4.1)[56,57] was used for this study. In all calculations, real-space projectors were used (LREAL = AUTO in VASP) and a plane-wave basis set for the electronic density, which incorporated reciprocal lattice vectors with a norm up to 3/2 times larger than for the wave function, $|\mathbf{G}_{cut}|$(PREC = Normal in VASP). An SCF-convergence criterion of $<10^{-8}$ eV was applied to the total energy, with a geometry convergence criterion of <0.005 eV/Å for the maximum norm of individual atomic forces.

The lattice constants of α-Fe_2O_3 were optimized, obtaining values ($a = b = 5.053$ Å and $c = 13.824$ Å) that agree well with experimental results ($a = b = 5.035$ Å and $c = 13.747$ Å).[58] The values also agree with the GGA + U computational results from prior studies: $a = b = 5.067$ Å, $c = 13.882$ Å.[25]

Surfaces were modeled with symmetric slabs containing nine formula units of Fe_2O_3 per dry (1×1) surface (approximately 19 Å thick), along with slabs of equivalent thickness for other terminations. These slabs were separated by a minimum of 24 Å of vacuum to reduce artificial interactions among periodic structures. A Γ-centered k-point grid with $(4 \times 4 \times 1)$ k-points for a (1×1)-α-$Fe_2O_3(0001)$ cell and $(2 \times 2 \times 1)$ k-points for (2×2) cells was used to sample the Brillouin zone of surfaces using a Gaussian smearing with $\sigma = 0.1$ eV.

RESULTS AND DISCUSSION

α-Fe_2O_3 crystallizes in the corundum bulk structure, where the oxygen atoms form a hexagonal closed-packed structure (AB-stacking) in which two-thirds of the octahedral voids are filled with metal ions. In the 0001 direction, each layer contains three O^{2-} ions and two Fe^{3+} ions. The two metal ions in one layer are not identical and occupy the three possible octahedral positions alternately and can therefore be described as ABC stacking. Therefore, the unit cell consists of six O_3-Fe_2 layers. The antiferromagnetic order for Fe in α-Fe_2O_3 is "++, −−" by layers along the 0001 direction.[25,59]

The stability of all surfaces is studied according to the Gibbs free energy of formation relative to the dry surface according to the reaction equation

$$\text{slab}_{dry} + x\text{Fe}_2\text{O}_3 + m\text{H}_2\text{O} \rightarrow \text{slab} + \frac{n}{2}\text{O}_2 \quad (1)$$

Here, x, m, and n are the stoichiometry coefficients which are defined for all given surfaces in Table 1. The surface free energy γ is then calculated from the Gibbs free energy of formation relative to the dry surface, per surface area A. The Gibbs free energy is approximated as the energy shifted by the chemical potential of the gas phase species (H_2O and O_2)

Table 1. Cell Size and Stoichiometry Coefficients x, m and n for the Studied Surfaces According to Equation 1

label	x	m	n	cell size
$\theta[Fe(OH)_3] = 0$ (dry/clean)	0	0	0	1×1
$\theta[Fe(OH)_3] = 1/4$	1	3	0	2×2
$\theta[Fe(OH)_3] = 1$	1	3	0	1×1
$\theta[H_2O] = 1$	0	2	0	1×1
$\theta[Fe(OH)_2] = 1/4$	1	2	1	2×2
$\theta[Fe(OH)_2] = 1$	1	2	1	1×1
$\theta[FeOH] = 1$	1	1	2	1×1
$\theta[FeO] = 1$	1	0	1	1×1

$$\gamma = \frac{E^{slab} - E^{slab}_{dry} - xE^{bulk}_{Fe_2O_3} - m[E^{gas}_{H_2O} + \mu_{H_2O}] + n[E^{gas}_{O_2}/2 + \mu_O]}{2A} \quad (2)$$

Here, E^{slab} and E^{slab}_{dry} are the energies of the slab models of the considered surface and of the dry surface with identical surface area A, $E^{bulk}_{Fe_2O_3}$ is the energy per formula unit of bulk α-Fe_2O_3. The surface area per (1×1) cell for α-Fe_2O_3 is $A = 22.110$ Å^2. The energy per bulk formula unit $E^{bulk}_{Fe_2O_3}$ was determined as the energy difference between two clean (1×1)-slabs differing by one Fe_2O_3-layer and this energy was used in all calculations. Computing the energy difference $E^{bulk}_{Fe_2O_3}$ for different unit cells or terminations resulted in negligible variations, approximately around 0.001 eV.

The chemical potential of water μ_{H_2O} is given relative to the energy of water $E^{gas}_{H_2O}$ and the chemical potential of oxygen μ_O is given relative to half of the energy of the O_2 molecule in its triplet ground state $E^{gas}_{O_2}/2$. The stoichiometry coefficients x, m, and n are determined by the amount of additional Fe, H, and O atoms on the surface with respect to the dry surface and are provided in Table 1.

In agreement with previous work[1,11,12,15,60,61] and same as for α-Al_2O_3,[26,45,62−64] we found that the most stable dry surface for α-Fe_2O_3 is a (1×1) surface that is terminated by a single Fe, i.e., (O_3-Fe). Figure 1 shows both a top view and a side-on view of this surface. Additionally, the labeling of both Fe- and O-layers is introduced in Figure 1, which will be used to refer to individual layers. Table 2 shows how the computed interlayer spacings obtained after relaxation with DFT deviate from the bulk limit. The topmost Fe atom in the first layer strongly relaxes downward, which reduces the distance between the Fe-layer and the lower oxygen layer by −65.3% of the corresponding interlayer spacing of the bulk so that the interlayer spacing at the surface is 34.7% of that of the bulk value. This is somewhat more than reported in previous work (−57%).[25] We note that the corresponding relaxation of the first layer is even stronger for α-$Al_2O_3(0001)$, where computed values range from −82 to −88%.[26,45,55]

The magnetic moments of the Fe atoms in the near-surface layers are compiled in Table S 3. The magnetic moments in the first (−4.00 μ_B) and second (+4.14 and +4.17 μ_B) layers differ slightly from the bulk value (±4.16 μ_B), to which the magnetic moments converge in the third layer (labeled layer "C" in Table 2). This is in good agreement with the literature (GGA + U),[25] where the magnetic moment of Fe is ±4.11 μ_B in the bulk, ± 3.94 μ_B in the first surface layer, and ±4.10 μ_B in the second surface layer. The experimental value is ±4.6−4.9 μ_B[65,66] for Fe in the bulk.

https://doi.org/10.1021/acsomega.4c02113
ACS Omega 2024, 9, 35449−35457

Table 2. Percent Change ($d\%\Delta$) in Layer Spacing from the α-Fe_2O_3 Relative to the Bulk Limit

		θ[Fe(OH)$_3$]		
$d\%\Delta$	dry	θ = 1/4	θ = 1	θ [H_2O] = 1
O_B–Fe^2_A		7.6	7.7	
Fe^2_A–Fe^1_A		73.1	−26.8	
Fe^1_A–O_A	−65.3	−55.2	9.6	−17.3
O_A–Fe^2_B	7.8	4.0	0.2	10.1
Fe^2_B–Fe^1_B	−37.3	−30.4	2.8	−28.9
Fe^1_B–O_B	16.2	14.2	−1.0	10.6
O_B–Fe^2_C	4.2	4.7	−0.5	0.7
Fe^2_C–Fe^1_C	−5.1	−5.3	1.1	1.4
Fe^1_C–$O_{A'}$	1.6	1.8	−0.2	−0.5
$O_{A'}$–$Fe^2_{A'}$	−0.9	−0.6	0.2	−0.5
$Fe^2_{A'}$–$Fe^1_{A'}$	2.7	2.1	−0.2	1.2
$Fe^1_{A'}$–$O_{B'}$	−0.5	−0.3	0.2	−0.2
$O_{B'}$–$Fe^2_{B'}$	0.3	0.2	0.0	0.2
$Fe^2_{B'}$–$Fe^1_{B'}$	−0.5	−0.2	0.2	0.0
$Fe^1_{B'}$–$O_{A''}$	0.4	0.3	0.1	0.3

Table 3. Mean Magnetic Moments (in μ_B) of the Upper Half Layers from the Slabs for the Relevant Reduced α-Fe_2O_3(0001) Surface Terminations[a]

			θ[Fe(OH)$_2$]	
	θ[FeO] = 1	θ[FeOH] = 1	θ = 1/4	θ = 1
Fe^2_A	−3.67	−3.62	−3.73	−3.71
Fe^1_A	−4.06	−3.64	−4.07	−4.13
Fe^2_B	+4.15	+4.16	+4.14	+4.15
Fe^1_B	+4.15	+4.16	+4.17	+4.16
Fe^2_C	−4.16	−4.16	−4.15	−4.16
Fe^2_C	−4.16	−4.16	−4.16	−4.16
$Fe^2_{A'}$	+4.16	+4.16	+4.16	+4.16
$Fe^1_{A'}$	+4.16	+4.16	+4.16	+4.16
$Fe^2_{B'}$	−4.16	−4.16	−4.16	−4.16
$Fe^1_{B'}$	−4.16	−4.16	−4.16	−4.16

[a]The magnetic moment is averaged over all Fe atoms belonging to the respective layer. The computed magnetic value of the bulk is μ = ± 4.16.

We will now discuss the hydroxylated surfaces of α-Fe_2O_3(0001). As for α-Al_2O_3,[55,67,68] the hydroxylated structures have been investigated for α-Fe_2O_3[31,36−39,43,50,60,69−71] both computationally and experimentally. One of the simplest hydroxylated structures results from the dissociative adsorption of water on the dry surface (θ[H_2O] = 1) (see Figure 2a). As for α-Al_2O_3,[26] the barrier for this dissociation was found to be very low (<0.1 eV) also for α-Fe_2O_3.[15]

The fully hydroxylated surface is terminated by a complete layer of oxygen that is saturated with one hydrogen per oxygen giving an OH concentration of 3 per (1 × 1) cell or 13.6 per nm^2. We find that there are structures with one or two of the three hydrogens pointing in a direction parallel to the surface and engaging in hydrogen bonding. As in previous work on α-Fe_2O_3(0001)[44] and α-Al_2O_3(0001),[72] we find the difference in stability to be negligible (≤0.05 eV) and only show in Figure 2b the structure with one in-plane hydrogen bond. As one may expect, MD simulations on α-Al_2O_3(0001) show that OH groups are not confined to these rigid positions.[73]

Comparing the termination of the dry surface (O_3–Fe) and that of the fully hydroxylated surface (Fe_2–(OH)$_3$), these two

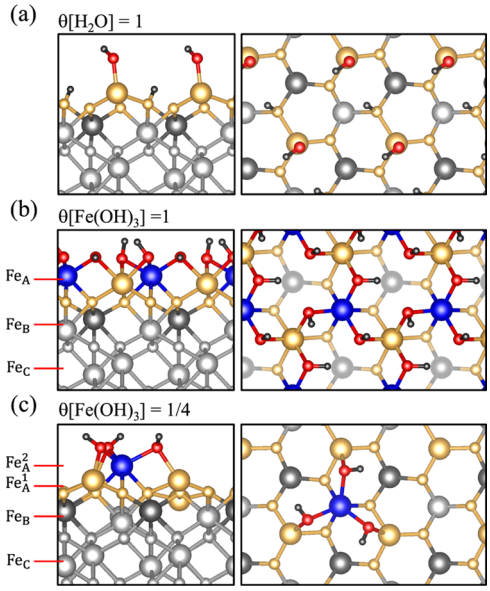

Figure 2. Atomic structure of hydroxylated surfaces. (a) Surface configuration with one H_2O molecule dissociated on top of the Fe-terminated Fe_2O_3(0001) (dry) surface. (b) Surface with θ[Fe(OH)$_3$] = 1. (c) Surface with θ[Fe(OH)$_3$] = 1/4. H, O, and Fe atoms are shown as small, medium, and large spheres, respectively. H atoms are shown in black, while a different color code is used to differentiate between the different layers for Fe (blue, gold, dark gray, light gray) and O (red, gold, light gray).

surfaces always differ by $\frac{3}{2}H_2O$ and $\pm Fe_2O_3$. So, one can think of it as one Fe(OH)$_3$ group adsorbed per (1 × 1) cell of the dry surface. Importantly, these Fe(OH)$_3$ groups are most stable, when adsorbed in the positions corresponding to a continuation of the bulk positions expected for Fe. Therefore, as in our previous work on α-Al_2O_3(0001),[45] we use the coverage of Fe(OH)$_3$ to describe the degree of hydroxylation of the surface. Here, θ[Fe(OH)$_3$] = 1 corresponds to the fully hydroxylated surface. The computed structures for θ[Fe(OH)$_3$] = 1 and 1/4 surfaces are shown in Figure 2.

The surface characterized by θ[Fe(OH)$_3$] = 1/4 contains an isolated Fe (OH)$_3$ fragment adsorbed on the dry surface. By isolated, we mean that Fe atoms in the layer below the top Fe(OH)$_3$ groups bind at most to one hydroxyl group (Figure 2c).[45]

Figure 3 shows the stability of the investigated surfaces as a function of the chemical potential of water, μ_{H_2O}. The surface resulting from dissociative water adsorption on the dry surface (θ[H_2O] = 1) is at no point the most stable structure. At high values of μ_{H_2O}, the fully hydroxylated surface θ[Fe(OH)$_3$] = 1 is most stable, while at low values of μ_{H_2O}, the dry surface θ[Fe(OH)$_3$] = 0 is most stable. Figure 3a shows that the θ[Fe(OH)$_3$] = 1/4 surface becomes more stable than the fully hydroxylated surface for $\mu_{H_2O} \leq -0.95$ eV, for example, at around 400 K and 1 mbar H_2O pressure. Dehydroxylation and the formation of the clean surface are only predicted to appear at $\mu_{H_2O} \leq -2.22$ eV, for example, at 850 K and 1 mbar H_2O pressure or at 700 K and 0.001 mbar H_2O pressure (see Figure 3b). Figure 3b has been obtained by considering only the loss of translational and rotational entropy associated with the reaction of H_2O(g), which is the leading contribution to adsorption at high temperatures. When vibrations are included,

https://doi.org/10.1021/acsomega.4c02113
ACS Omega 2024, 9, 35449−35457

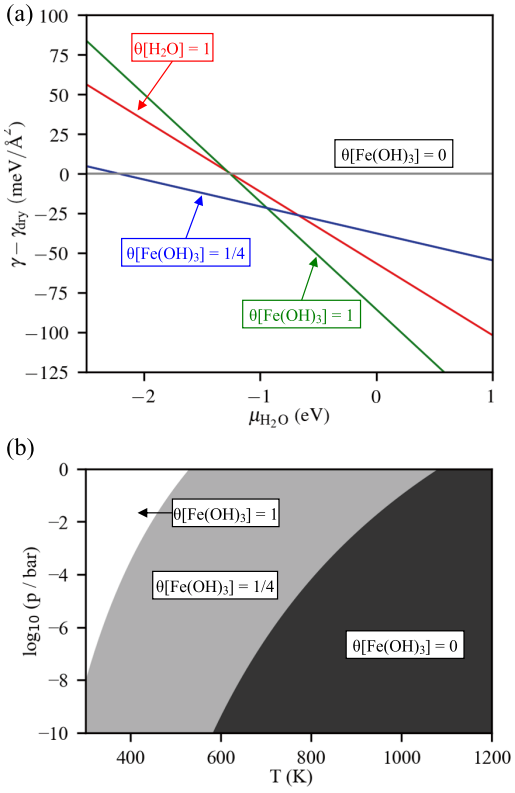

Figure 3. Stability of α-$Fe_2O_3(0001)$ surfaces. (a) Surface free energies are given relative to the dry surface as a function of the chemical potential of water μ_{H_2O}. (b) Phase diagram as a function of temperature and the partial pressure of water.

similar results are obtained (Figure S4). As one may expect, the main effect of considering the vibrational entropy of the surface is a stabilization of the hydroxyl groups at higher temperatures. The effect is largest for the transition from $\theta[Fe(OH)_3] = 1/4$ to the dry surface in the temperature range of 600−1200 K. However, it is not clear how good the harmonic approximation is at these elevated temperatures, since it cannot describe the full motion of hydroxyl groups. The main effect of zero-point vibrational energies is to disfavor hydroxylation by approximately 0.13 eV per $Fe(OH)_3$ group.

Compared to the calculations with $U = 4$ eV, the results with $U = 3$ and 5 eV are similar, with more (less) favorable hydroxylation predicted for 5 (3) eV (see Figure S2). The chemical potential of H_2O, where the transitions that occur are shifted at most by 0.1 eV. We thus concluded that the predicted stability of nonreduced hydroxylated and clean surfaces depends only weakly on the value of U.

Tables 2 and S3 list the surface relaxation and magnetic moments, respectively. The deviation of the interlayer spacing from the bulk is comparable for most hydroxylated surfaces, but is clearly the smallest for the fully hydroxylated surface, $\theta[Fe(OH)_3] = 1$. This can be explained by the fact the termination by OH groups is most similar to a bulk-like layer of oxygens. The magnetic moment converges in all cases quickly to the bulk limit with comparable deviations in the first two layers (<0.2 μ_B). To investigate how the reactivity of the partially hydroxylated surface with $\theta[Fe(OH)_3] = 1/4$ differs from the dry and the fully hydroxylated surfaces, we considered CO and H_2O as probe molecules, absorbed at a low coverage of $\theta = 1/4$. We find that the binding energy on the partially hydroxylated surface is intermediate between dry and fully hydroxylated surface (see the SI for details).

We will now briefly discuss how the stability of the α-$Fe_2O_3(0001)$ surface compares with the results obtained for α-$Al_2O_3(0001)$ in previous work.[45] This is of interest because the two are iso-structural and the results obtained for α-$Fe_2O_3(0001)$ are significantly different. In both cases, surfaces with low hydroxyl group concentration are stable, but for α-$Al_2O_3(0001)$ this stability extends to much lower values of μ_{H_2O} and it is not obvious why. In Figure 3, we have, as in previous work, given the surface energy relative to the dry surface ($\gamma_{dry} = 0$). This choice is motivated by the fact that the absolute stability of the dry surface is irrelevant to determine which termination is most stable under certain conditions. However, to compare the 0001 surface of the α-Fe_2O_3 and α-Al_2O_3, we found it useful to employ the absolute surface energies. For comparison, it is additionally useful to give the surface energy not per area, but per (1×1) unit cell, because this leads to the same concentration of hydroxyl groups

$$\gamma = \frac{E^{slab} - \frac{x}{2}E^{bulk}_{M_2O_3} - m[E^{gas}_{H_2O} + \mu_{H_2O}] + n[E^{gas}_{O_2}/2 + \mu_O]}{2A} \times A_{1\times1} \quad (3)$$

As opposed to eq 2, in eq 3, all Fe is referenced to bulk α-Fe_2O_3 and x therefore simply equals the number of metal ions in the slab. The absolute surface energies per unit cell are given in Figure 4.

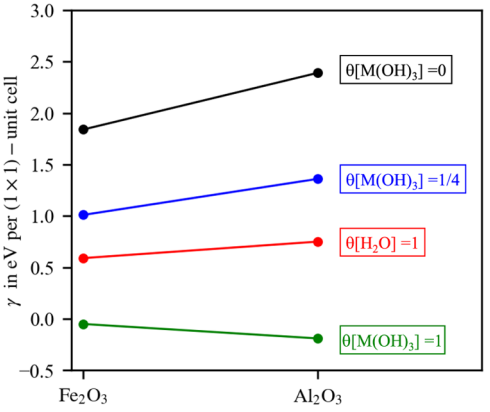

Figure 4. Absolute surface energies per unit cell computed according to eq 3 with data for α-$Al_2O_3(0001)$ taken from previous work.[45]

It can be seen in Figure 4 that the total surface energies of the fully hydroxylated surface, $\theta[M(OH)_3] = 1$, varies only slightly, with values of −0.05 and −0.19 per unit cell for Fe_2O_3 and Al_2O_3, respectively. Note that this corresponds to the 0 K ($\mu(H_2O) = 0$) surface energies. Negative surface energies for hydroxylated surfaces at 0 K have been computed before, for α-$Al_2O_3(0001)$,[55] θ-$Al_2O_3(110)$,[74,75] and α-quartz(0001).[75,76] The small absolute value and small variation of these surface energies can be explained by the fact that all metal atoms retain their octahedral coordination when the fully hydroxylated surface is formed from the bulk. Furthermore, the number of hydroxyl groups also stays constant when the hydroxylated surface is created through the reaction with H_2O.

The stability of the dry surface, $\theta[M(OH)_3] = 0$ varies strongly from α-Fe_2O_3 to α-Al_2O_3, from 1.84 to 2.39 eV per unit cell. The dry surface and fully hydroxylated surface have the same stability for α-$Al_2O_3(0001)$ when the chemical

https://doi.org/10.1021/acsomega.4c02113
ACS Omega 2024, 9, 35449−35457

potential of water is $\mu(H_2O) = -1.72$ eV.[45] The much more stable dry surface of α-$Fe_2O_3(0001)$ leads to an earlier crossover at $\mu(H_2O) = -1.26$ eV (Figure 3). Consequently, the lower stability of fully hydroxylated surface $\theta[M(OH)_3] = 1$ observed in Figure 3 for α-$Fe_2O_3(0001)$ is mainly due to the more stable dry surface.

For the partially hydroxylated surface with $\theta[M(OH)_3] = 1/4$, Figure 4 shows an increase in surface energy from 1.03 to 1.36 eV per unit cell when going from Fe_2O_3 to Al_2O_3. Compared to the stability of α-$Al_2O_3(0001)$ surfaces, both $\theta[Fe(OH)_3] = 1/4$ and $\theta[Fe(OH)_3] = 1$ surfaces are relatively less stable than their corresponding alumina structures. Similar to α-$Al_2O_3(0001)$ surfaces,[45] it is possible that there is a large variety of structures between $\theta[Fe(OH)_3] = 1/4$ and $\theta[Fe(OH)_3] = 1$, such as $\theta[Fe(OH)_3] = 4/9$.

We will now discuss reduced structures, which contain Fe in the oxidation state +2. The motivation for considering surface reduction is that we believe reduction of hematite to magnetite to begin at the surface, in this case, α-$Fe_2O_3(0001)$. One interesting question is that if surface reduction is more or less favorable than bulk reduction. As above, we will describe the structures in terms of the group that is adsorbed on the dry surface and its respective coverage. The most stable obtained structures can be derived from the hydroxylated structures discussed above (Fe in oxidation state +3) by removing an OH group. Removing an OH group from $\theta[Fe(OH)_3] = 1/4$ and $\theta[Fe(OH)_3] = 1$, results in the structures labeled $\theta[Fe(OH)_2] = 1/4$ and $\theta[Fe(OH)_2] = 1$. Here, the topmost Fe is in oxidation state +2 as evidenced by the magnetic moment, see Table S3. Further removal of an OH group gives $\theta[Fe(OH)] = 1$, in which both top Fe ions are in oxidation state +2. The reduced surface $\theta[FeO] = 1$ can be obtained by removing H_2O from $\theta[Fe(OH)_2] = 1$.

The atomic structure of the reduced surfaces is shown in Figure 5, and the phase diagram in Figure 6 summarizes all relevant structures. Figure 6a shows the phase diagram as the function of the chemical potentials of oxygen and water. At the top of the phase diagram, for chemical potentials of oxygen $\mu_O < -1.5$ eV, only nonreduced surfaces without Fe^{2+} (also displayed in Figure 3) are stable. The stability of the reduced surfaces is generally a function of the chemical potentials of both water and oxygen. The reduced structures with low hydroxyl concentration ($\theta[FeO] = 1$ and $\theta[Fe(OH)] = 1$) are only stable in a range of chemical potentials $\mu_O < -2.44$ eV, where bulk hematite is less stable than bulk magnetite, according to experimental data.[77] The only reduced surfaces in the phase diagram that extend to higher values of μ_O are $\theta[Fe(OH)_3] = 1$ and $\theta[Fe(OH)_2] = 1/4$. We also note that the chemical potential of oxygen at which calculations predict this transition is usually lower, ranging from −1.60 to −1.73 eV for PBE + U with $0 < U < 5$ eV, as opposed to the experimental value of $\mu_O < -2.44$ eV.[51] Consequently, the first formation of reduced surfaces is predicted by our calculations at a similar potential at which DFT + U also predicts (erroneously) the transition from bulk hematite to bulk magnetite.[51] From this, we conclude that the formation of reduced α-$Fe_2O_3(0001)$ surface occurs in a similar range of the chemical potential of μ_O as the reduction of bulk hematite to bulk magnetite. This is of course only a thermodynamic analysis and one can speculate that surface reduction of hematite is kinetically more facile than complete reduction of bulk hematite to magnetite. Figure S3 shows the results obtained for $U = 3$ and 5 eV in addition to those depicted in Figure 6. A higher U value (5 eV) generally leads to easier reduction and vice versa for a lower U value (3 eV). This shifts the phase boundaries systematically by about 0.2 eV (see Figure S3).

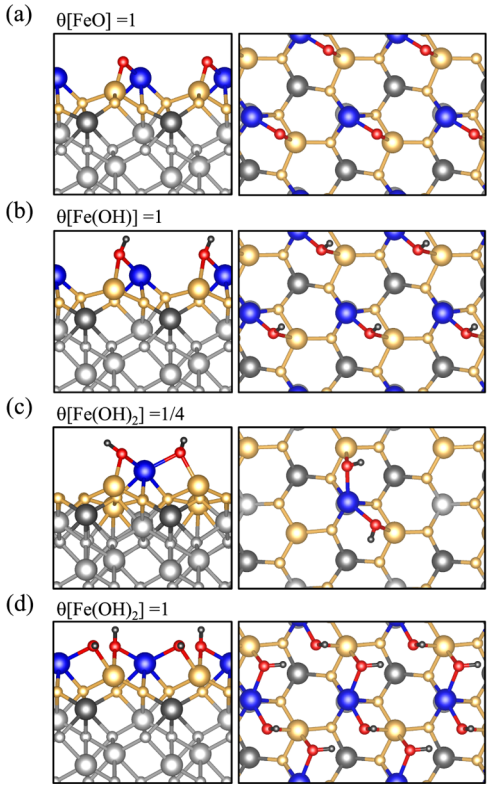

Figure 5. Atomic structure of reduced surfaces of α-$Fe_2O_3(0001)$ with the same color code as in Figure 2 for surfaces with (a) $\theta[FeO] = 1$, (b) $\theta[Fe(OH)] = 1$, (c) $\theta[Fe(OH)_2] = 1/4$, and (d) $\theta[Fe(OH)_2] = 1$.

In Figure 6b, we show the stability of the same phases as a function of the chemical potential of hydrogen and water. The transformation is achieved simply by using the experimental formation energy of water and setting $\mu_O = -2.476$ eV + $\mu_{H_2O} - \mu_{H_2}$. Under oxidizing conditions, Figure 6a is a more useful representation, while Figure 6b is more convenient to analyze the stability under reducing conditions. Both of these situations are relevant for a potential process,[9] in which iron is used as a solid fuel, that is burned (with O_2) to yield hematite and is then reduced (using H_2) to again give iron.

SUMMARY AND CONCLUSIONS

Hydroxylated terminations of the α-$Fe_2O_3(0001)$ surface were studied using PBE + U calculations. In addition to previously investigated, fully hydroxylated structures, we found that structures with a low concentration of hydroxyl groups are stable at relatively low chemical potentials of water. Here, low concentration means at least 3 times lower than the fully hydroxylated surface, which has three OH groups per (1×1) cell. These surfaces can be described as isolated $Fe(OH)_3$ groups adsorbed on the dry 0001 surface of hematite and they are identical in structure to the previously investigated surface of α-$Al_2O_3(0001)$.[45]

In addition to surfaces with Fe only in oxidation state +3, oxidized and reduced terminations were also investigated. In agreement with previous work, oxidized surfaces are not found to be stable at relevant conditions. Many of the investigated

https://doi.org/10.1021/acsomega.4c02113
ACS Omega 2024, 9, 35449−35457

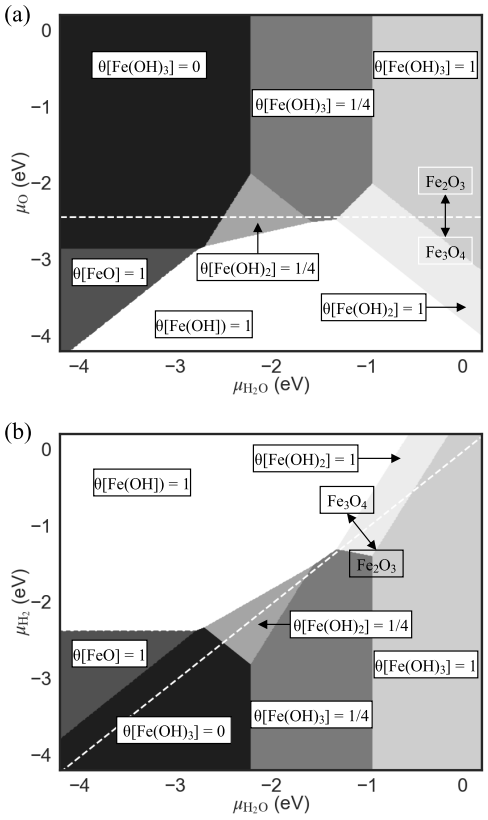

Figure 6. Phase diagram for α-Fe_2O_3(0001) surface terminations (a) as a function of the chemical potential of water μ_{H_2O} and oxygen μ_O. The range of stability of bulk hematite and bulk magnetite is indicated based on experimental values.[77] The horizontal dashed line indicates the chemical potential at which the transition occurs. Phase diagram for α-Fe_2O_3(0001) surface terminations (b) as a function of μ_{H_2O} and chemical potential of hydrogen μ_{H_2}.

reduced surfaces only become stable at chemical potentials of oxygen, $\mu_O < -2.44$ eV, where bulk hematite is unstable with respect to reduction to bulk magnetite. The only reduced surfaces stable in a range of $\mu_O > -2.44$ eV are those derived from hydroxylated surfaces, where OH groups are removed. Given the fact that PBE + U predicts a too early reduction of hematite to magnetite (at too high values of μ_O), these results suggest that reduced surfaces of hematite are thermodynamically only stable in a range, where bulk hematite is less stable than bulk magnetite.

The predicted stability of hydroxylated surfaces with low OH concentration is expected to be not very sensitive to methodology, based on our previous investigation of α-Al_2O_3(0001).[45] In particular, the stability of these structures is very similar for values of U = 3, 4, and 5 eV. The prediction of oxidation/reduction behavior depends more strongly on methodology, for example, the employed value of U. Here, a higher value of U (5 eV) leads to slightly easier reduction, while a lower value of U (3 eV) makes reduction less favorable. The precise value of the chemical potential of oxygen, μ_O, where reduction of the surface takes place is thus not determined with high confidence. Here, higher levels of theory would be required to make more reliable predictions.

Overall, the structures investigated in this work, which contain a low concentration of hydroxyl groups are predicted to be the most stable surfaces in a wide range of chemical potentials of water -0.95 eV > μ_{H_2O} > -2.22 eV. This means that only at high chemical potentials (for example, in liquid water) or at very low chemical potentials (for example, in UHV and at high temperatures), other surfaces are most stable (fully hydroxylated and clean, respectively). The knowledge of the atomic structure of surfaces is the prerequisite for making predictions of their properties and reactivity using first-principles calculations. Consequently, the surface terminations proposed in this work are important for most future studies on hematite surfaces since many experimental conditions are in the relevant range.

■ ASSOCIATED CONTENT

Supporting Information

The Supporting Information is available free of charge at https://pubs.acs.org/doi/10.1021/acsomega.4c02113.

Total energies and Cartesian coordinates of all involved structures (PDF)

Structures (TXT)

■ AUTHOR INFORMATION

Corresponding Author

Philipp N. Plessow − *Institute of Catalysis Research and Technology, Karlsruhe Institute of Technology, 76344 Eggenstein-Leopoldshafen, Germany;* orcid.org/0000-0001-9913-4049; Email: plessow@kit.edu

Authors

Jiachen Chen − *Institute of Catalysis Research and Technology, Karlsruhe Institute of Technology, 76344 Eggenstein-Leopoldshafen, Germany;* orcid.org/0000-0002-9654-4947

Dmitry I. Sharapa − *Institute of Catalysis Research and Technology, Karlsruhe Institute of Technology, 76344 Eggenstein-Leopoldshafen, Germany;* orcid.org/0000-0001-9510-9081

Complete contact information is available at: https://pubs.acs.org/10.1021/acsomega.4c02113

Notes

The authors declare no competing financial interest.

■ ACKNOWLEDGMENTS

The authors acknowledge support by the state of Baden-Württemberg through bwHPC and the German Research Foundation (DFG) through grant no. INST 40/575-1 FUGG (JUSTUS 2 cluster). J.C. and P.N.P. acknowledge funding by the Deutsche Forschungsgemeinschaft (DFG, German Research Foundation)−SFB 1441−Project-ID 426888090. This work was also supported by the DFG under project GRK 2450. Financial support from the Helmholtz Association is also gratefully acknowledged.

■ REFERENCES

(1) Parkinson, G. S. Iron oxide surfaces. *Surf. Sci. Rep.* **2016**, *71*, 272−365.

(2) Sivula, K.; Le Formal, F.; Grätzel, M. Solar water splitting: Progress using hematite (α-Fe_2O_3) photoelectrodes. *ChemSusChem* **2011**, *4*, 432−449.

(3) Zandi, O.; Hamann, T. W. The potential versus current state of water splitting with hematite. *Phys. Chem. Chem. Phys.* **2015**, *17*, 22485−22503.

(4) Wang, H.; Chen, T.; Liu, H.; Li, W.; Zou, X.; Wang, C.; Li, M. Comprehensive Application of Oolitic Hematite for H_2S Removal at High Temperature: Performance and Mechanism. *Energy Fuels* **2019**, *33*, 2037−2044.
(5) Albrecht, M.; Rodemerck, U.; Schneider, M.; Bröring, M.; Baabe, D.; Kondratenko, E. V. Unexpectedly efficient CO_2 hydrogenation to higher hydrocarbons over non-doped Fe_2O_3. *Appl. Catal., B* **2017**, *204*, 119−126.
(6) Yang, Q.; Kondratenko, V. A.; Petrov, S. A.; Doronkin, D. E.; Saraçi, E.; Lund, H.; Arinchtein, A.; Kraehnert, R.; Skrypnik, A. S.; Matvienko, A. A.; Kondratenko, E. V. Identifying Performance Descriptors in CO_2 Hydrogenation over Iron-Based Catalysts Promoted with Alkali Metals. *Angew. Chem., Int. Ed.* **2022**, *61*, No. e202116517.
(7) Skrypnik, A. S.; Petrov, S. A.; Kondratenko, V. A.; Yang, Q.; Lund, H.; Matvienko, A. A.; Kondratenko, E. V. Descriptors Affecting Methane Selectivity in CO_2 Hydrogenation over Unpromoted Bulk Iron(III)-Based Catalysts. *ACS Catal.* **2022**, *12*, 11355−11368.
(8) Yang, Q.; Kondratenko, V. A.; Skrypnik, A. S.; Lund, H.; Bartling, S.; Weiss, J.; Brückner, A.; Kondratenko, E. V. Understanding of the Fate of α-Fe_2O_3 in CO_2 Hydrogenation through Combined Time-Resolved In Situ Characterization and Microkinetic Analysis. *ACS Catal.* **2023**, *13*, 9064−9077.
(9) Debiagi, P.; Rocha, R. C.; Scholtissek, A.; Janicka, J.; Hasse, C. Iron as a sustainable chemical carrier of renewable energy: Analysis of opportunities and challenges for retrofitting coal-fired power plants. *Renewable Sustainable Energy Rev.* **2022**, *165*, No. 112579.
(10) Ali, M. L.; Fradet, Q.; Riedel, U. Kinetic Mechanism Development for the Direct Reduction of Single Hematite Pellets in H_2/CO Atmospheres. *Steel Res. Int.* **2022**, *93*, No. 2200043.
(11) Barbier, A.; Stierle, A.; Kasper, N.; Guittet, M. J.; Jupille, J. Surface termination of hematite at environmental oxygen pressures: Experimental surface phase diagram. *Phys. Rev. B* **2007**, *75*, No. 233406.
(12) Wang, X. G.; Weiss, W.; Shaikhutdinov, S. K.; Ritter, M.; Petersen, M.; Wagner, F.; Schlögl, R.; Scheffler, M. The hematite (α-Fe_2O_3) (0001) surface: Evidence for domains of distinct chemistry. *Phys. Rev. Lett.* **1998**, *81*, 1038−1041.
(13) Kiejna, A.; Pabisiak, T. Mixed termination of hematite (α-Fe_2O_3)(0001) surface. *J. Phys. Chem. C* **2013**, *117*, 24339−24344.
(14) Bergermayer, W.; Schweiger, H.; Wimmer, E. Ab initio thermodynamics of oxide surfaces: O_2 on Fe_2O_3(0001). *Phys. Rev. B* **2004**, *69*, No. 195409.
(15) Nguyen, M. T.; Seriani, N.; Gebauer, R. Water adsorption and dissociation on α-Fe_2O_3(0001): PBE+U calculations. *J. Chem. Phys.* **2013**, *138*, No. 194709.
(16) Ovcharenko, R.; Voloshina, E.; Sauer, J. Water adsorption and O-defect formation on Fe_2O_3(0001) surfaces. *Phys. Chem. Chem. Phys.* **2016**, *18*, 25560−25568.
(17) Pabisiak, T.; Kiejna, A. Fe adsorption on hematite (α-Fe_2O_3) (0001) and magnetite (Fe_3O_4) (111) surfaces. *J. Chem. Phys.* **2014**, *141*, No. 134707.
(18) Stirner, T.; Scholz, D.; Sun, J. Ab initio simulation of structure and surface energy of low-index surfaces of stoichiometric α-Fe_2O_3. *Surf. Sci.* **2018**, *671*, 11−16.
(19) Redondo, J.; Michalička, J.; Kraushofer, F.; et al. Hematite α-Fe_2O_3(0001) in Top and Side View: Resolving Long-Standing Controversies about Its Surface Structure. *Adv. Mater. Interfaces* **2023**, *10*, No. 2300602.
(20) Yang, Y.; Ma, H.; Zhuang, J.; Wang, X. Morphology-controlled synthesis of hematite nanocrystals and their facet effects on gas-sensing properties. *Inorg. Chem.* **2011**, *50*, 10143−10151.
(21) Huang, X.; Hou, X.; Zhang, X.; Rosso, K. M.; Zhang, L. Facet-dependent contaminant removal properties of hematite nanocrystals and their environmental implications. *Environ. Sci. Nano* **2018**, *5*, 1790−1806.
(22) Guo, Y.; Clark, S. J.; Robertson, J. Electronic and magnetic properties of Ti_2O_3, Cr_2O_3, and Fe_2O_3 calculated by the screened exchange hybrid density functional. *J. Phys.: Condens. Matter* **2012**, *24*, No. 325504.
(23) Pozun, Z. D.; Henkelman, G. Hybrid density functional theory band structure engineering in hematite. *J. Chem. Phys.* **2011**, *134*, No. 224706.
(24) Mosey, N. J.; Carter, E. A. Ab initio evaluation of Coulomb and exchange parameters for DFT+U calculations. *Phys. Rev. B* **2007**, *76*, No. 155123.
(25) Rohrbach, A.; Hafner, J.; Kresse, G. Ab initio study of the (0001) surfaces of hematite and chromia: Influence of strong electronic correlations. *Phys. Rev. B* **2004**, *70*, No. 125426.
(26) Hass, K. C.; Schneider, W. F.; Curioni, A.; Andreoni, W. The chemistry of water on alumina surfaces: Reaction dynamics from first principles. *Science* **1998**, *282*, 265−268.
(27) Dudarev, S. L.; Liechtenstein, A. I.; Castell, M. R.; Briggs, G. A. D.; Sutton, A. P. Surface states on NiO (100) and the origin of the contrast reversal in atomically resolved scanning tunneling microscope images. *Phys. Rev. B* **1997**, *56*, No. 4900.
(28) Dudarev, S. L.; Botton, G. A.; Savrasov, S. Y.; Humphreys, C. J.; Sutton, A. P. Electron-energy-loss spectra and the structural stability of nickel oxide: An LSDA+U study. *Phys. Rev. B* **1998**, *57*, No. 1505.
(29) Liechtenstein, A. I.; Anisimov, V. I.; Zaanen, J. Density-functional theory and strong interactions: Orbital ordering in Mott-Hubbard insulators. *Phys. Rev. B* **1995**, *52*, No. R5467(R).
(30) Anisimov, V. I.; Aryasetiawan, F.; Lichtenstein, A. I. First-principles calculations of the electronic structure and spectra of strongly correlated systems: the LDA+ U method. *J. Phys.: Condens. Matter* **1997**, *9*, No. 767.
(31) Wang, R. B.; Hellman, A. Initial water adsorption on hematite (α-Fe_2O_3) (0001): A DFT + U study. *J. Chem. Phys.* **2018**, *148*, No. 094705.
(32) Lewandowski, M.; Groot, I. M.; Qin, Z. H.; Ossowski, T.; Pabisiak, T.; Kiejna, A.; Pavlovska, A.; Shaikhutdinov, S.; Freund, H. J.; Bauer, E. Nanoscale Patterns on Polar Oxide Surfaces. *Chem. Mater.* **2016**, *28*, 7433−7443.
(33) Ossowski, T.; Pabisiak, T.; Kiejna, A.; Palotás, K.; Bauer, E. Simulation of STM Images of Hematite α-Fe_2O_3(0001) Surfaces: Dependence on Distance and Bias. *J. Phys. Chem. C* **2021**, *125*, 26711−26717.
(34) Lemire, C.; Bertarione, S.; Zecchina, A.; Scarano, D.; Chaka, A.; Shaikhutdinov, S.; Freund, H. J. Ferryl (Fe = O) termination of the Hematite α-Fe_2O_3(0001) surface. *Phys. Rev. Lett.* **2005**, *94*, No. 166101.
(35) Sterrer, M.; Freund, H. J. Towards realistic surface science models of heterogeneous catalysts: Influence of support hydroxylation and catalyst preparation method. *Catal. Lett.* **2013**, *143*, 375−385.
(36) Yamamoto, S.; Kendelewicz, T.; Newberg, J. T.; Ketteler, G.; Starr, D. E.; Mysak, E. R.; Andersson, K. J.; Ogasawara, H.; Bluhm, H.; Salmeron, M.; Brown, G. E.; Nilsson, A. Water adsorption on α-Fe_2O_3 (0001) at near ambient conditions. *J. Phys. Chem. C* **2010**, *114*, 2256−2266.
(37) Schöttner, L.; Ovcharenko, R.; Nefedov, A.; Voloshina, E.; Wang, Y.; Sauer, J.; Wöll, C. Interaction of Water Molecules with the α-Fe_2O_3(0001) Surface: A Combined Experimental and Computational Study. *J. Phys. Chem. C* **2019**, *123*, 8324−8335.
(38) Yin, S.; Ma, X.; Ellis, D. E. Initial stages of H2O adsorption and hydroxylation of Fe-terminated α-Fe_2O_3(0001) surface. *Surf. Sci.* **2007**, *601*, 2426−2437.
(39) Souvi, S. M.; Badawi, M.; Paul, J. F.; Cristol, S.; Cantrel, L. A DFT study of the hematite surface state in the presence of H_2, H_2O and O_2. *Surf. Sci.* **2013**, *610*, 7−15.
(40) English, N. J.; Rahman, M.; Wadnerkar, N.; Macelroy, J. M. Photo-active and dynamical properties of hematite (Fe_2O_3)-water interfaces: An experimental and theoretical study. *Phys. Chem. Chem. Phys.* **2014**, *16*, 14445−14454.
(41) Von Rudorff, G. F.; Jakobsen, R.; Rosso, K. M.; Blumberger, J. Hematite(001)-liquid water interface from hybrid density functional-based molecular dynamics. *J. Phys.: Condens. Matter* **2016**, *28*, No. 394001.

https://doi.org/10.1021/acsomega.4c02113
ACS Omega 2024, 9, 35449−35457

(42) Trainor, T. P.; Chaka, A. M.; Eng, P. J.; Newville, M.; Waychunas, G. A.; Catalano, J. G.; Brown, G. E. Structure and reactivity of the hydrated hematite (0001) surface. *Surf. Sci.* **2004**, *573*, 204−224.
(43) Pabisiak, T.; Kiejna, A. Incipient adsorption of water and hydroxyl on hematite (0001) surface. *J. Phys. Commun.* **2019**, *3*, No. 035023.
(44) Liao, P.; Keith, J. A.; Carter, E. A. Water oxidation on pure and doped hematite (0001) surfaces: Prediction of Co and Ni as effective dopants for electrocatalysis. *J. Am. Chem. Soc.* **2012**, *134*, 13296−13309.
(45) Chen, J.; Sharapa, D.; Plessow, P. N. Stability and formation of hydroxylated α-Al_2O_3(0001) surfaces at high temperatures. *Phys. Rev. Res.* **2022**, *4*, No. 013232.
(46) Perdew, J. P.; Burke, K.; Ernzerhof, M. Generalized Gradient Approximation Made Simple. *Phys. Rev. Lett.* **1996**, *77*, No. 3865.
(47) Rohrbach, A.; Hafner, J.; Kresse, G. Electronic correlation effects in transition-metal sulfides. *J. Phys.: Condens. Matter* **2003**, *15*, 979−996.
(48) Grimme, S.; Antony, J.; Ehrlich, S.; Krieg, H. A consistent and accurate ab initio parametrization of density functional dispersion correction (DFT-D) for the 94 elements H-Pu. *J. Chem. Phys.* **2010**, *132*, No. 154104.
(49) Cococcioni, M.; de Gironcoli, S. Linear response approach to the calculation of the effective interaction parameters in the LDA+U method. *Phys. Rev. B* **2005**, *71*, No. 035105.
(50) Huang, X.; Ramadugu, S. K.; Mason, S. E. Surface-Specific DFT + U Approach Applied to α-Fe_2O_3(0001). *J. Phys. Chem. C* **2016**, *120*, 4919−4930.
(51) Meng, Y.; Liu, X. W.; Huo, C. F.; Guo, W. P.; Cao, D. B.; Peng, Q.; Dearden, A.; Gonze, X.; Yang, Y.; Wang, J.; Jiao, H.; Li, Y.; Wen, X. D. When Density Functional Approximations Meet Iron Oxides. *J. Chem. Theory Comput.* **2016**, *12*, 5132−5144.
(52) Schöttner, L.; Ovcharenko, R.; Nefedov, A.; Voloshina, E.; Wang, Y.; Sauer, J.; Wöll, C. Interaction of Water Molecules with the a-Fe2O3(0001) Surface: A Combined Experimental and Computational Study. *J. Phys. Chem. C* **2019**, *123*, 8324−8335.
(53) Wang, R. B.; Hellman, A. Surface terminations of hematite (α-Fe_2O_3) exposed to oxygen, hydrogen, or water: dependence on the density functional theory methodology. *J. Phys.: Condens. Matter* **2018**, *30*, No. 275002.
(54) Ruscic, B.; Bross, D. H. Active Thermochemical Tables (ATcT) values based on ver. 1.122 of the Thermochemical Network 2016. http://ATcT.anl.gov.
(55) Wang, X. G.; Chaka, A.; Scheffler, M. Effect of the environment on α-Al_2O_3 (0001) surface structures. *Phys. Rev. Lett.* **2000**, *84*, No. 3650.
(56) Kresse, G.; Joubert, D. From ultrasoft pseudopotentials to the projector augmented-wave method. *Phys. Rev. B* **1999**, *59*, No. 1758.
(57) Kresse, G.; Furthmüller, J. Efficient iterative schemes for ab initio total-energy calculations using a plane-wave basis set. *Phys. Rev. B* **1996**, *54*, No. 11169.
(58) Finger, L. W.; Hazen, R. M. Crystal structure and isothermal compression of Fe_2O_3, Cr_2O_3, and V_2O_3 to 50 kbars. *J. Appl. Phys.* **1980**, *51*, 5362−5367.
(59) Rollmann, G.; Rohrbach, A.; Entel, P.; Hafner, J. First-principles calculation of the structure and magnetic phases of hematite. *Phys. Rev. B* **2004**, *69*, No. 165107.
(60) Wasserman, E.; Rustad, J. R.; Felmy, A. R.; Hay, B. P.; Halley, J. W. Ewald methods for polarizable surfaces with application to hydroxylation and hydrogen bonding on the (012) and (001) surfaces of α-Fe_2O_3. *Surf. Sci.* **1997**, *385*, 217−239.
(61) Lübbe, M.; Moritz, W. A LEED analysis of the clean surfaces of α-Fe_2O_3(0001) and α-Cr_2O_3(0001) bulk single crystals. *J. Phys.: Condens. Matter* **2009**, *21*, No. 134010.
(62) Łodziana, Z.; Nørskov, J. K.; Stoltze, P. The stability of the hydroxylated (0001) surface of α-Al_2O_3. *J. Chem. Phys.* **2003**, *118*, 11179−11188.
(63) Batyrev, I.; Alavi, A.; Finnis, M. W. Ab initio calculations on the Al_2O_3(0001) surface. *Faraday Discuss.* **1999**, *114*, 33−43.
(64) Guo, J.; Ellis, D. E.; Lam, D. J. Electronic structure and energetics of sapphire (0001) and (1 $\bar{1}$02) surfaces. *Phys. Rev. B* **1992**, *45*, 13647−13656.
(65) Krén, E.; Szabó, P.; Konczos, G. Neutron diffraction studies on the (1-x) Fe_2O_3 - xRh_2O_3 system. *Phys. Lett.* **1965**, *19*, 103−104.
(66) Coey, J. M. D.; Sawatzky, G. A. A study of hyperfine interactions in the system $(Fe_{1-x}Rh_x)_2O_3$ using the Mossbauer effect (Bonding parameters). *J. Phys. C: Solid State Phys.* **1971**, *4*, No. 2386.
(67) Ranea, V. A.; Carmichael, I.; Schneider, W. F. DFT Investigation of Intermediate Steps in the Hydrolysis of α-Al_2O_3(0001). *J. Phys. Chem. C* **2009**, *113*, 2149−2158.
(68) Thissen, P.; Grundmeier, G.; Wippermann, S.; Schmidt, W. G. Water adsorption on the α-Al_2O_3(0001) surface. *Phys. Rev. B* **2009**, *80*, No. 245403.
(69) Liu, P.; Kendelewicz, T.; Brown, G. E.; Nelson, E. J.; Chambers, S. A. Reaction of water vapor with α-Al_2O_3(0001) and α-Fe_2O_3(0001) surfaces: synchrotron X-ray photoemission studies and thermodynamic calculations. *Surf. Sci.* **1998**, *417*, 53−65.
(70) Kurtz, R. L.; Henrich, V. E. Surface electronic structure and chemisorption on corundum transition-metal oxides: α-Fe_2O_3. *Phys. Rev. B* **1987**, *36*, No. 3413.
(71) Hellman, A.; Pala, R. G. First-principles study of photoinduced water-splitting on Fe_2O_3. *J. Phys. Chem. C* **2011**, *115*, 12901−12907.
(72) Mason, S. E.; Iceman, C. R.; Tanwar, K. S.; Trainor, T. P.; Chaka, A. M. Pb(II) adsorption on isostructural hydrated alumina and hematite (0001) surfaces: A DFT Study. *J. Phys. Chem. C* **2009**, *113*, 2159−2170.
(73) Wirth, J.; Saalfrank, P. The Chemistry of Water on α-Alumina: Kinetics and Nuclear Quantum Effects from First Principles. *J. Phys. Chem. C* **2012**, *116*, 26829−26840.
(74) Łodziana, Z.; Topsøe, N. Y.; Nørskov, J. K. A negative surface energy for alumina. *Nat. Mater.* **2004**, *3*, 289−293.
(75) Goumans, T. P. M.; Wander, A.; Brown, W. A.; Catlow, C. R. A. Structure and stability of the (001) α-quartz surface. *Phys. Chem. Chem. Phys.* **2007**, *9*, 2146−2152.
(76) Plessow, P. N.; Sánchez-Carrera, R. S.; Li, L.; Rieger, M.; Sauer, S.; Schaefer, A.; Abild-Pedersen, F. Modeling the Interface of Platinum and α-Quartz(001): Implications for Sintering. *J. Phys. Chem. C* **2016**, *120*, 10340−10350.
(77) *CRC Handbook of Chemistry and Physics*, 85th ed.; Lide, D. R., Ed.; CRC Press, 2004.

https://doi.org/10.1021/acsomega.4c02113
ACS Omega 2024, 9, 35449−35457